Desalination 580 (2024) 117513

Contents lists available at ScienceDirect

Desalination

journal homepage: www.elsevier.com/locate/desal

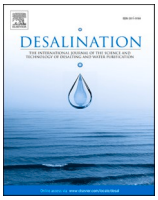

Novel spacer geometries for membrane distillation mixing enhancement

Alaa Adel Ibrahim *, Marie-Alix Dalle, Filip Janasz, Stephan Leyer

Department of Engineering, University of Luxembourg, 6 Rue Richard Coudenhove-Kalergi, 1359 Kirchberg, Luxembourg

HIGHLIGHTS

- CFD simulation of a channel filled with spacers in MD systems.
- Spacer geometry effect on the mixing performance and heat transfer.
- Mixer geometry spacers exhibit a pronounced ability to enhance flow turbulence effectively.
- Spiral geometry spacers show minimal pressure drop, requiring less pumping power.

ARTICLE INFO

Keywords:
MD
Desalination
Spacers
CV
Mixing
Heat transfer

ABSTRACT

Membrane distillation is an emerging promising desalination method that requires further improvement in order to become industrially viable. Due to the fact that evaporation is the primary process in membrane distillation, one strategy to boost membrane permeate flux is to optimize the energy supply to the water interface by increasing mixing in the hot channel via the use of optimized spacers. Contemporary spacer designs predominantly induce turbulence, resulting in elevated pumping energy requirements. This study introduces novel spacer geometries, inspired by industrial mixer designs, to surmount the limitations of conventional spacer configurations. The mixing efficiency, thermal performance, and pressure drop induced by the two novel geometries are studied and compared to those of commonly utilized spacer designs. It is confirmed, that the first of these novel geometries significantly enhances mixing, whereas the other causes a lower pressure drop and appears to be a viable solution when a spacer is a necessary structural component. In the course of the analysis, it is also shown that the coefficient of variation coupled with the Nusselt number at the membrane can be used to assess spacers' performance.

1. Introduction

Membrane distillation (MD) is a non-isothermal water desalination method that utilizes a selective membrane barrier and combines membrane-based and thermal desalination technologies. This technique involves the passage of exclusively vapor molecules through a porous hydrophobic membrane, which is strategically positioned between a feed solution maintained at a higher temperature and a permeate stream maintained at a lower temperature [1]. MD is developing as a viable alternative method for water desalination and treatment. In comparison to reverse osmosis (RO) and conventional thermal desalination, the MD process is more cost-effective and efficient in terms of product purity because it requires less heat [2].

The two predominant configurations of MD, namely direct contact membrane distillation (DCMD) and air-gap membrane distillation (AGMD), have gained major relevance. In AGMD, in contrast to DCMD, an air gap is introduced between the membrane and the coolant stream, thereby mitigating heat losses (see Fig. 1).

MD is based on evaporation, which depends on the heat transfer towards the membrane in the hot water channel. In the MD process, the temperature difference between the hot water membrane interface and the cold flow induces evaporation and consequently freshwater production. Increasing the heat transfer rate to the interface, vapor diffusion in the air-gap, and condensation processes all improve MD output flow. However, MD faces technical challenges such as temperature polarization and membrane fouling/scaling, which can impede efficiency or cause operational issues [3].

The thermal gradient between the module's hot and cold channels decreases proportionally with the distance traveled along the membrane from the inlet. Therefore, the driving force of evaporation diminishes,

* Corresponding author.
E-mail address: alaa.ibrahim@uni.lu (A.A. Ibrahim).

https://doi.org/10.1016/j.desal.2024.117513
Received 13 November 2023; Received in revised form 4 March 2024; Accepted 7 March 2024
Available online 12 March 2024

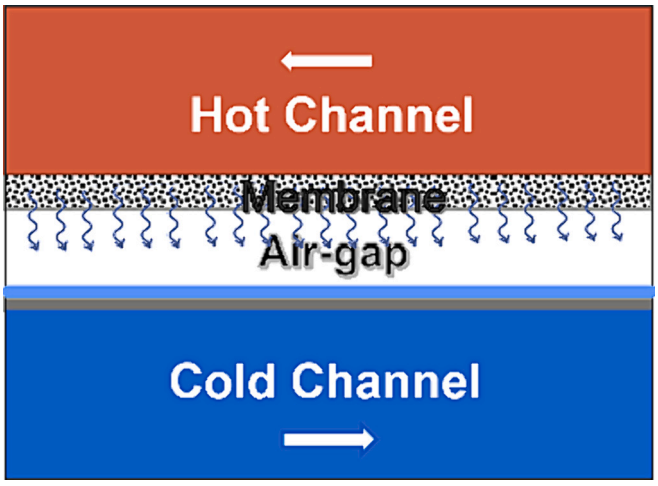

Fig. 1. Schematic diagram of typical AGMD process.

resulting in a reduction in the freshwater output. There are various strategies available for mitigating temperature polarization in MD. Passive techniques encompass the incorporation of spacers, utilization of corrugated membrane surfaces, and employing specialized membrane fabrication methods (e.g., nanostructured membranes, nanoheated membranes, metallic membranes [4]). On the other hand, active approaches involve surface vibration, flow vibration, ultrasonic fields, or membrane heating [5].

Fouling is a membrane failure common in MD, involves the accumulation of species from the feed solution on the membrane surface, blocking its pores and diminishing water vapor flux, potentially leading to pore wetting. It is caused by the deposition of contaminants like salts, minerals, or organic matter, both on the membrane surface and within its pores, resulting in clogged pores during MD operations. This lowers the flow of latent heat of water vaporization, reducing membrane lifetime [3]. In addressing fouling/scaling in MD, besides primary methods, advanced strategies have emerged, including nanobubble injection inducing turbulent flow in the feed channel [6], utilizing spacers to promote turbulence, and enhancing superhydrophobic or omni phobic membranes to augment surface roughness [7].

From an energy efficiency standpoint, passive techniques are preferred. In particular, spacers are attractive due to their ease of use and design flexibility. Spacers are widely used in MD as a turbulence promoter [8]. In fact, they have two additional major roles: providing support for the membrane [9] and reducing fouling due to the hydrophobic nature of the membrane [10].

Within a laminar flow regime, the transfer of heat occurs from the bulk water phase to the interface through the process of heat diffusion, which is less efficient than convection. On the other hand, inducing turbulences results in an increased convective transfer and is a straightforward technique to maintain high temperatures at the membrane, while increasing shear rate at the membrane surface through fluid deflection and promoting turbulent flow to prevent solute concentration build-up, consequently inhibiting foulant layer formation [33]. Nevertheless, with the escalation of flow kinetic energy losses and drag, there is a corresponding rise in the pressure drop along the channel. As a result, additional pumping energy is required [11], which may result in membrane wetting due to the liquid entry pressure being exceeded. Achieving this balance necessitates considering the advantages of enhanced mixing against the potential drawbacks of membrane wetting and increased pumping energy consumption [9].

Numerical investigations were utilized in order to examine the system performance in AGMD and to analyze the system performance by adjusting the membrane porosity at various inlet feed temperatures (Tfeed) in counter-current and co-current flow regimes [12]. It is also confirmed that AGMD systems produce better thermal performance than DCMD thanks to the numerical analysis modeling the coupled heat and mass transfer in [13]. Zhaoguang Xu et al.'s CFD simulation [14] utilizing an established heat and mass transport model to investigate the AGMD process for NaCl solution.

The most common type of spacer is the net type, composed of fibers arranged in a crisscrossing pattern. Parameters controlling these types of spacers' performance include: (1) the angle formed by the liquid's direction and the net mesh, (2) the voidage [11], (3) the angle between the fibers forming the net, (4) the spacer mesh aspect ratio (Conventional commercial spacers typically feature a square mesh pattern, whereas customized spacers can be designed with two distinct length parameters [15]), (5) the overall spacer's thickness, and (6) the fibers cross-section size and shape [16].

Several studies in the literature have focused on optimizing spacer geometry for MD processes. Seo et al. [17] conducted a comprehensive analysis of 51 different spacer combinations and geometries, determining that an asymmetric, circular zig-zag spacer design with thicker and more numerous fibers maximizes freshwater output while minimizing pressure drop with thinner fibers and lower fiber count. Chernyshov [16], proposed two configurations, either circular cross-section fibers arranged perpendicularly with the entire net placed at a 45^0 angle to the flow, or twisted tape fibers forming an angle of 30^0 with the flow and 120^0 between fibers, to achieve the lowest pressure drop and extensive mixing. The placement of net-type spacers in the MD module has been identified as a critical parameter affecting performance. *Al*-Sharif et al. [18] utilized a custom model implemented in OpenFOAM to investigate pressure drop and temperature polarization with different circular cross-section fibers net-type spacer configurations at various distances from the membrane surface. Similarly, Shakaib et al. [19] explored the impact of the placement of circular cross-section fibers net-type spacers in the channel on temperature polarization, revealing that a stagnant water layer occurs at the membrane interface when fibers are perpendicular to the flow direction, leading to enhanced temperature polarization and reduced shear stress at the membrane. These findings collectively contribute valuable insights for the optimization of spacer design and placement in MD systems.

To enhance spacer performance, various studies have explored modifying fiber cross-sections. Dendukuri et al. [20] found that altered fiber shapes can result in a 45 % higher pressure drop compared to conventional circular fibers. Ni et al. [21] showed that a net-type spacer with curved crossings enhanced heat transfer but also led to a significantly larger pressure drop. Li et al. [5] proposed two novel fiber shapes, with the twisted tape fiber in a multilayer structure outperforming conventional spacers. Armbruster et al. [22] reported that shortening twisted tape spacers reduces pressure drop and specific dissipated energy, making twisted tape geometry a promising choice based on available literature.

Beyond net-type spacers, alternative methodologies exist to enhance flow mixing. Other solutions are utilized in many technical applications, including industrial water treatment and the oil industry [23], for purposes such as gas dissolution, solid dissolution, polymer dissolution, and heat homogenization. Overall, a mix of both active and passive methods is used in the industrial sector. Energy is required for dynamic mixing, which is usually done with rotating blades. On the contrary, passive elements positioned in the flow channel, referred to as static mixers (SM) can split, twist, and recombine streams [24], to produce an extensional flow. Compared to shear flow induced by spacers it consumes more power while mixing equally well [25].

Various geometries have been explored to enhance mixing in cylindrical pipelines, with the Kenics-type mixer and LPD (low pressure drop) mixer standing out for their low-induced pressure drop [26]. Liu et al. [27] introduced a novel spacer geometry for spiral-wound MD devices, utilizing SM techniques to move fluid layers within the channel. The experiments demonstrated slightly superior mass transfer coefficients (<10 %) compared to conventional spacers Due to the emerging

capabilities afforded by 3D printing [28], Thomas et al. ([29,30]) introduced novel spacer configurations rooted in triply periodic minimal surfaces—a mathematical construct recognized for its efficacy in minimizing dead zones and facilitating laminar flow, thereby efficiently mitigating fouling. In a parallel investigation, Armbruster et al. [31] conducted experiments involving a Kenics mixer geometry, which bears a notable resemblance to the twisted tape spacer geometry, alongside eight alternative twisted tape configurations. These experiments demonstrated a pronounced reduction in fouling in the context of MD.

Both Kenics and LPD-type static mixers (SM) are recognized for efficiently promoting flow mixing. Since literature already covers Kenics-type spacers, this study will focus on deriving a novel spacer geometry using LPD. Furthermore, it is noteworthy that the Kenics geometry is similar to the twisted tape configuration.

In this work, the most promising spacer geometries identified above were used as a basis to design and generate two three-dimensional models. The first replicates twisted tape/Kenics type, while the other is the LPD type. Extrapolating from the reviewed literature, these designs have a promise of increased mixing performance while minimizing associated pressure losses. To validate this, numerical simulations using CFD software were performed, where novel designs were compared against typical and commonly used spacers. However, there are numerous means to assess the mixing performance, requiring varied degrees of analysis effort. Therefore, in parallel to spacer geometry validation, an investigation has been made to compare and find the most suitable performance indicators.

2. Methodology

2.1. Measures of spacers performance

The most important parameters describing the efficiency of a spacer are the mixing efficiency, the generated pressure drop, and thermal performance represented in Nusselt number (*Nu*).

In the context of spacer investigation in MD, the primary metric utilized to evaluate mixing efficiency is the Sherwood number, which quantifies the relationship between convective and diffusive mass transfer processes. This parameter is formally defined as:

$$Sh = \frac{k_m L}{D} \tag{1}$$

where k_m denotes the mass transfer coefficient, L is a characteristic distance, and D represents mass diffusivity. Nevertheless, several empirical correlations have been proposed to determine this value. As an example, for a rectangular slit with a height H, Lévêque [32] recommends:

$$Sh = 1.467\left(Re\frac{\nu}{D}\frac{H}{L}\right)^{\frac{1}{3}} \tag{2}$$

Here *Re* represents the Reynolds number, ν tands for the kinematic viscosity, and *L* denotes the length of the channel. In reference [5], the Sherwood formula is used with k_m defined as:

$$k_m = \frac{1}{A}\oint_A \frac{1}{C_{bulk} - C_{wall}}\left(-D\frac{\delta C}{\delta y}\right)_{wall} \tag{3}$$

A being the area of membrane.

The application of the Lévêque equation [32] was extended by Shrivstava et al. [28] to encompass 2D spacer geometries beyond a rectangular slit. This extension was based on the assumption that when the fluid encounters a new spacer barrier, its concentration rapidly achieves uniform distribution, similar to how a uniform mixture behaves when it enters a new tube. The spacer is divided into rectangular blocks, with good agreement in simple cases. However, predictions for complex geometries like herringbones or helical spacers are more uncertain due to complex flows. For novel spacers creating 3D velocity fields, rectangular block discretization isn't suitable. Therefore, relying on the adapted Lévêque equation with the Shrivstava procedure carries some risk.

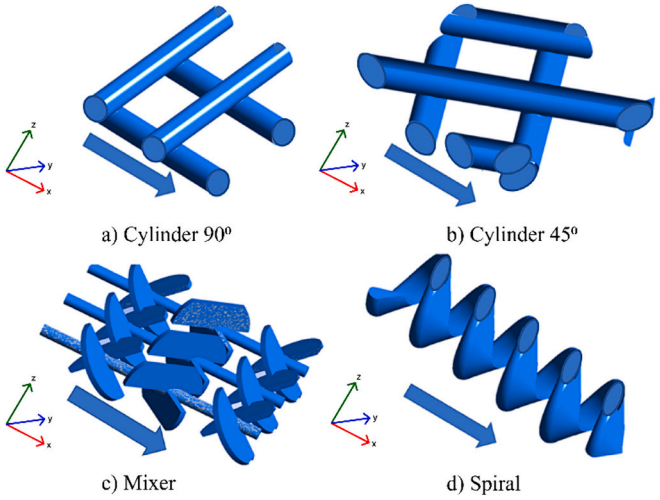

Fig. 2. Geometries of the investigated spacers. The blue arrows indicate the direction of the flow. (For interpretation of the references to colour in this figure legend, the reader is referred to the web version of this article.)

In this study, the degree of homogeneity in mixing within the hot channel can be evaluated through the utilization of the coefficient of variation (CV). It is a statistical measure that represents the relative variability or dispersion of a dataset in relation to its mean. In this study CV is calculated for dye mass fraction by dividing the standard deviation of the dye mass fraction by the mean and expressing the result as a percentage. As the CV approaches 0, it signifies a high degree of homogeneity, indicating that the fluid is thoroughly mixed. Conversely, as the CV approaches 1, it implies a lower degree of homogeneity, indicating that the fluid is not properly mixed. Consequently, a reduced CV implies a thoroughly blended mixture.

In industrial applications, the CV is often used as a measure of mixture homogeneity. To evaluate the performance of a novel static mixer designed by *Al*-Atabi [33], experiments were conducted to determine the CV pertaining to the mixing of two streams of Newtonian fluids. Additionally, Bennour et al. conducted a numerical investigation into the mixing phenomenon induced by various baffles within a static mixer [34]. By combining both empirical experimentation and computational fluid dynamics (CFD) analysis, the CV was utilized as a quantifiable measure of mixing degree to comprehensively assess the homogeneity of mixtures in two distinct types of static mixers [35].

Hence, in this study, the CV will serve as a straightforward indicator of mixing quality, easily computed from numerically derived data.

Another important measure of spacer performance is the flow energy dissipation. It can be assessed by measuring the pressure drop as follows:

$$dP = 4f\left(\frac{L}{D_e}\right)\rho\frac{u^2}{2} \tag{4}$$

Here, ρ presents the fluid density, *L* is the channel length, D_e stands for the equivalent hydraulic diameter of the channel, $f = \frac{A}{Re^n}$ denotes the friction factor, and *u* is the flow velocity.

In this work the pressure drop *dP* is calculated directly from the obtained numerical results by averaging and subtracting static pressures over two planes in the calculation domain. The planes are located before and after the spacer and are perpendicular to the inlet velocity.

Moreover, the Nusselt number (*Nu*) is utilized to indicate the enhanced heat transfer resulting from the fluid motion, the average *Nu* on the membrane surface can be defined as:

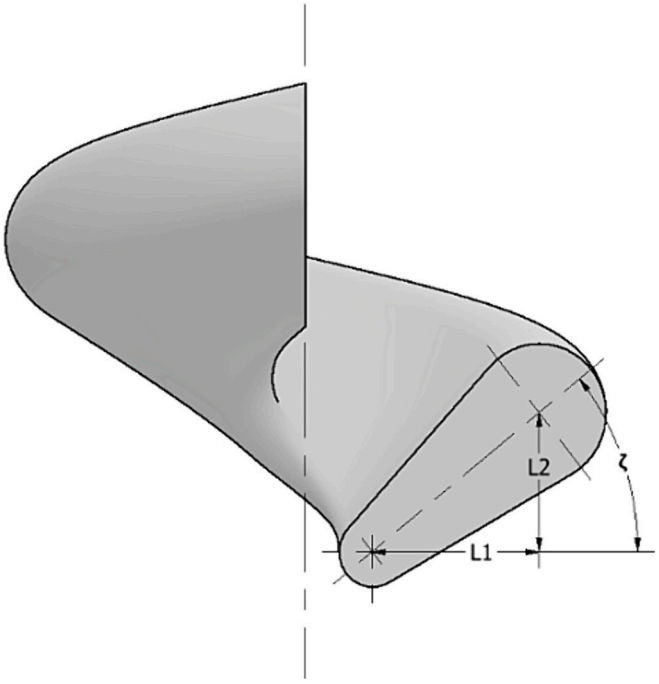

Fig. 3. Cross-section of the spiral geometry. The ratio L1/L2 determines the wall inclination angle, ζ.

$$Nu = \frac{h_{ave}L}{k} \tag{5}$$

where the average convective heat transfer coefficient h_{ave},

$$h_{ave} = \frac{q_{ave}}{T_f - T_m} \tag{6}$$

In these equations, L is the characteristic length, k is the thermal conductivity of fluid, q_{ave} is the average heat flux, T_f is the fluid temperature, equals to 57 °C, and T_m is for the membrane surface temperature which is 27 °C.

2.2. Proposed novel spacer geometries

This study starts with a spiral configuration (referred to as spiral, Fig. 2 d), featuring a voidage of $\varepsilon_{spiral} = 0.948$. This design was developed based on the top-performing spacer identified in the literature review, namely the twisted tape, in combination with the Kenics mixer [26].

The second configuration is derived from an industrial SM LPD design, chosen for its ability to induce similarly low pressure drops (referred to as "mixer," depicted in Fig. 2 c), featuring a voidage of $\varepsilon_{mixer} = 0.939$.

For the purpose of numerical simulations, the membrane was located in the (x,y) plane, leaving (z) as a direction perpendicular to the membrane.

To benchmark the performance of novel spacer designs, a reference in the form of conventional standard spacer was defined as a net-type with circular cross-section fibers. Two positioning configurations were tested: one with fibers parallel and perpendicular to the flow (case *cylinder 90^0*, Fig. 2 a), and one at 45^0 from the flow(case cylinder 45^0, Fig. 2 b). In both cases, fibers were at 90^0 to each other, and aspect ratio is 1:1. The voidage of these two net-type spacers was the same, $\varepsilon_{cylinder} = 0.730$.

The thickness δ of all these spacers was set to δ = 5mm, and the calculation was defined around it, with walls remaining in contact with the spacers. This is the typical arrangement for AGMD modules where spacers are used to provide support.

Table 1
Spiral geometries parameters.

Spacer name	ζ [rad]	L1 [mm]	L2 [mm]	Revolutions
Spiral	0.78	1.5	1.5	4
SpiralB	0.78	1.5	1.5	6.67
SpiralC	0.78	1.5	1.5	5
SpiralD	0.92	1.5	2	4
SpiralE	1.03	1.5	2.5	4

Table 2
Physical properties of the working fluids.

Fluid properties (Water & Dye)	Value
Density, ρ (kg/m^3)	998.2
Dynamic viscosity, μ (kg/m·s)	0.001003
Thermal conductivity, k (W/m·K)	0.6
Mass diffusivity, D (m^2/s)	2.88e−50

In addition, as a reference case for all the tested spacer geometries, flow in an empty channel is calculated using the same boundary condition set (case empty).

The details of a particular implementation of a spacer design impact its performance. To investigate this effect a spiral geometry was chosen, and a few versions of it were produced (see Fig. 2). The variation included changed revolution and increased inclination of the side walls of the spiral (see Fig. 3: Cross-section of the spiral geometry).

The configurations spiralB and spiralC were created to study the influence of the spiral's revolution by adjusting the number of turns along the domain length. Additionally, the designs spiralD and spiralE were generated to assess the effect of the inclination angle (ζ) of the spiral walls. The variation is achieved by modifying the ratio of l_2/l_1. By increasing it, the angle grows, and spiral surfaces are more aligned with the flow direction (Fig. 3 and Table 1).

2.3. Numerical model description

Transient three-dimensional computational fluid dynamics (CFD) models are implemented using ANSYS Fluent software, ver 2022 R2. The shear-Stress Transport (SST) k-ω Model is used here to describe the turbulence within the fluid, and the pressure-based solver is employed to solve the complete set of the governing equations (see Appendix A.).

The coupling between pressure and velocity is accomplished through the implementation of the Semi-Implicit Method for Pressure Linked Equations (SIMPLE) algorithm.

Within the computational models, simulations, liquid water and a custom-defined dye with identical properties to water are utilized (see Table 2), with the dye acting as a tracer for calculating the Coefficient of Variation (CV). To investigate the mixing phenomenon, a species-transport model is selected, where the general form of the species transport equation is defined as:

$$\frac{\partial}{\partial t}(\rho Y_i) + \nabla \bullet (\rho \vec{v} Y_i) = -\nabla . \vec{J_i} + R_i + S_i \tag{7}$$

where the mass diffusion $\vec{J_i}$ for turbulent flow is given by:

$$\vec{J_i} = -\left(\rho D_{i,m} + \frac{\mu_t}{Sc_t}\right)\nabla Y_i - D_{T,i}\frac{\nabla T}{T} \tag{8}$$

Here, Y_i represents the local mass fraction of each species ι, R_i stands for the net rate of species production, S_i is the rate of creation by addition from the dispersed phase plus any source terms, Sc_t is the turbulent Schmidt number, μ_t is the turbulent, D_T and, D_m are the thermal and mass diffusion.

2.3.1. Computational domain and boundary conditions

This research introduces a computational investigation using three-

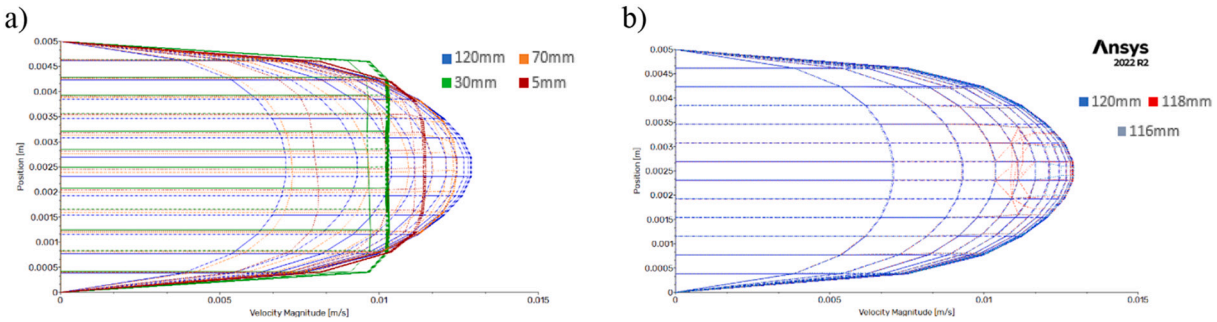

Fig. 4. Velocity profiles for the flow in the entrance length a) Developing region b) Fully developed velocity profiles.

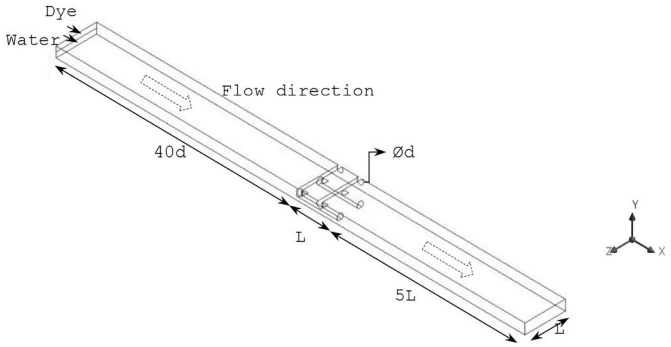

Fig. 5. Geometry of the computational domain.

dimensional numerical simulations to model and predict the impact of integrating the proposed spacer onto the membrane surface within an AGMD, specifically focusing on its effects on the mixing behavior and heat transfer characteristics.

The study evaluated five spacer arrangements (cylinder 90^0, cylinder 45^0, spiral, mixer, and empty) along with four different versions of the spiral configurations (refer to Table 1). These were subjected to a consistent set of boundary conditions.

The value mass diffusivity (D) in Table 2 is kept significantly lower than the actual value of the working fluids, in order to eliminate the effect of diffusion on mixing behavior and focus on the influence of the spacers.

The main parameter, inlet velocity, was varied between $V_{in} = 0.01$, 0.05, 0.1, and 0.25 m/s, encompassing a representative range observed in AMGD processes [36].

The size of the calculation domain is 0.24*0.02*0.005 m. The height was selected to replicate typical hot water channels in MD. The width was determined to ensure a minimum of 2 fibers in each direction for conventional spacers, and 3 elements in each direction for the mixer spacer. This measure was considered as a representative minimum characteristic element of the overall geometry. The minimum length of the domain should be sufficient to guarantee the proper placement of spacers within the fully developed region. Fig. 4 shows the analysis of the velocity profiles at the lowest inlet velocity of the working fluid. Fig. 4a displays velocity profiles of various planes located within the entrance length, revealing that full development of flow occurs at the plane located 120 mm from the entrance. In Fig. 4b, it is observed that velocity profiles repeat among planes situated just 2 mm apart from each other. As a result, in this study the length of the entry region is determined to be 40 times the diameter of the spacer (symbolized as d), with d being equivalent to 3 mm. The length of the region of interest is represented by L, while the outlet region, which is 5 times the length of the region of interest (5 L), is designated to minimize the impact of boundary effects.

Fig. 5 illustrates the geometric configuration of the computational domain, which was created using Inventor software. To investigate mixing, the domain's input surface was split evenly into two horizontal parts. This division, combined with the utilization of a species transport model incorporating a volume-weighted mixing law, facilitated the introduction of two distinct liquids through separate inlets, allowing for tracking of their mixing behavior. Both liquids were assigned the same inlet velocities. At the outlet, a pressure outlet boundary condition was set with a gauge pressure of 0 Pa, while the remaining surfaces were defined as wall boundaries with a no-slip condition. Initially, the simulations were adiabatic to investigate the mixing behavior influenced by the spacers, with the energy equation disabled. Subsequently, the energy equation was activated to examine the heat transfer behavior. The primary objective of this study involves the optimization of spacer geometry in order to minimize pressure losses, improve mixing characteristics, and enhance thermal performance. The investigation focuses on the flow behavior of various regimes with Reynolds numbers ranging from 80 to 1990. However, the conventional spacer has been previously assessed in literature at higher Reynolds numbers. Table 3 provides a summary of the boundary conditions for the cases examined in this study.

Table 3
Summary of boundary conditions.

	Material	Boundary condition	Model	Viscous
1. Mixing study numerical model (see Section 3.1)				
Inlet 1 Inlet 2	Water Dye	- Fixed velocity inlet: 0.01–0.25 m/s	- Species transport - Adiabatic	Shear-Stress Transport (SST) turbulence model
Bottom & top walls		- Stationary wall/ No slip		
Outlet		- Zero pressure		
2. Heat transfer study numerical model (see Section 3.2)				
Inlet	Water	- Fixed velocity inlet: 0.01–0.25 m/s - Temperature: 57 °C	Non-adiabatic model	Shear-Stress Transport (SST) turbulence model
Bottom wall		- Stationary wall/ No slip - Temperature: 27 °C		
Top wall		- Stationary wall/ No slip - Heat flux = 0		
Outlet		- Zero pressure		

2.3.2. Grid sensitivity study

The mesh generation process was carried out using Ansys Fluent, version 2022 R2, to create an appropriate mesh that can accurately capture the phenomena of mixing and heat transport resulting from the introduction of the proposed spacers. By confirming that the results are

Table 4
Mesh sensitivity study.

Geometry	No.	Number of elements	dP[pa]	%Change
Cylinder 90^0	M1	2,445,337	0.5716	–
	M2	3,367,696	0.5836	2.093 %
	M3	10,015,564	0.5860	0.410 %
Cylinder 45^0	M4	8,069,946	0.9531	–
	M5	10,973,146	0.9573	0.44 %
	M6	14,807,215	0.9589	0.1638 %
Spiral	M7	3,355,987	0.1382	–
	M8	4,891,579	0.1395	0.956 %
	M9	8,736,054	0.1412	1.230 %
Mixer	M10	3,322,526	0.7843	–
	M11	4,678,272	0.7922	0.9880 %
	M12	7,020,624	0.7982	0.7515 %
	M13	10,398,540	0.7998	0.1992 %

not excessively sensitive to the mesh, the study enhances the confidence in the accuracy and validity of the numerical solution.

Three grid systems are conducted for the geometries Cylinder 90^0, Cylinder 45^0, and Spiral. Four grid systems are conducted for the Mixer geometry. As it is obvious from.

Table 4, the generated grids exhibit non-significant variations in pressure drop values across the different cases. Based on this analysis, grids number M2, M5, M7, and M11 were chosen for the simulations corresponding to the four respective geometries. The selection was made due to the fact that the percentage change in pressure drop between the chosen grids and the larger grids was found to be <1 %, thus validating their suitability for the present simulations.

2.3.3. Model validation

The established CFD model undergoes validation through comparison with previously published numerical outcomes and experimental results conducted by Koutsou et al. [10], along with experimental data obtained by Schock and Miquel [37]. In Fig. 6, the relationship between pressure drop and flow velocity is displayed within a channel featuring crossed cylinder spacers at a 90^0 orientation, with a filament spacing-to-diameter ratio (l/d) of 6 and a flow contact angle of 90^0. The modeling results prove reasonable agreement with the established data.

Following the successful optimization of both the mathematical model and the validation of the computational fluid dynamics (CFD) model. It's appropriate to predict the effect of changing the geometrical characteristics of the spacers inside the feed channel, and their subsequent impact on mixing and thermal performance.

3. Results and discussion

With a focus on the impact of incorporating spacer filaments into the membrane of the hot channel within an AGMD system, this study examines how variations in their geometric design affect the system's performance in terms of mixing and heat transfer. The investigation covers a flow inlet velocity range of 0.01 m/s to 0.25 m/s. Numerical results and corresponding contour representations are obtained through the utilization of CFD simulation models, enabling a comparative analysis of different configurations.

3.1. Mixing study

3.1.1. Effect of spacer geometry on the mixing behavior, and pressure drop

Fig. 7 presents the Coefficient of Variation (CV) ratio for various spacer geometries in comparison to the empty channel, aiming to evaluate the mixing performance. The CV is calculated on three perpendicular planes to the flow direction, specifically at the endpoint (0 mm) of the spacer geometry, at 10 mm far from the spacer, and at 20 mm far from the spacer respectively.

Lower CV ratio indicates improved mixing compared to the empty channel. In this study, a significantly low value for the mass diffusivity (D) of the fluids was intentionally chosen (See Table 2). The purpose behind this selection is to suppress the influence of diffusivity on the mixing phenomena to focus only on assessing the impact of convective mixing induced by incorporating spacers with distinct geometries.

The results demonstrate that the inclusion of any spacer in the system significant enhances the mixing behavior, as evidenced by all ratios being <1. Notably, as the inlet velocity rises from 0.01 m/s to 0.25 m/s, the mixer geometry spacer exhibits the best mixing performance among the different spacer geometries at the end of the spacer with an average enhancement of 88 %. While the spiral spacer demonstrates the lowest degree of mixing as it has the highest CV ratio across all examined velocities, resulting in an average enhancement of 30 %. The average enhancement in mixing caused by the cylinder 90^0 and cylinder 45^0 spacers are 64 % and 48 % respectively.

Moving further away from the spacer (see Fig. 7b, c), it is notable that each spacer exhibits distinct turbulence behavior. Specifically, in the case of cylindrical spacers, mixing is notably affected by distance, with performance levels of 84 % and 89 % respectively observed after a

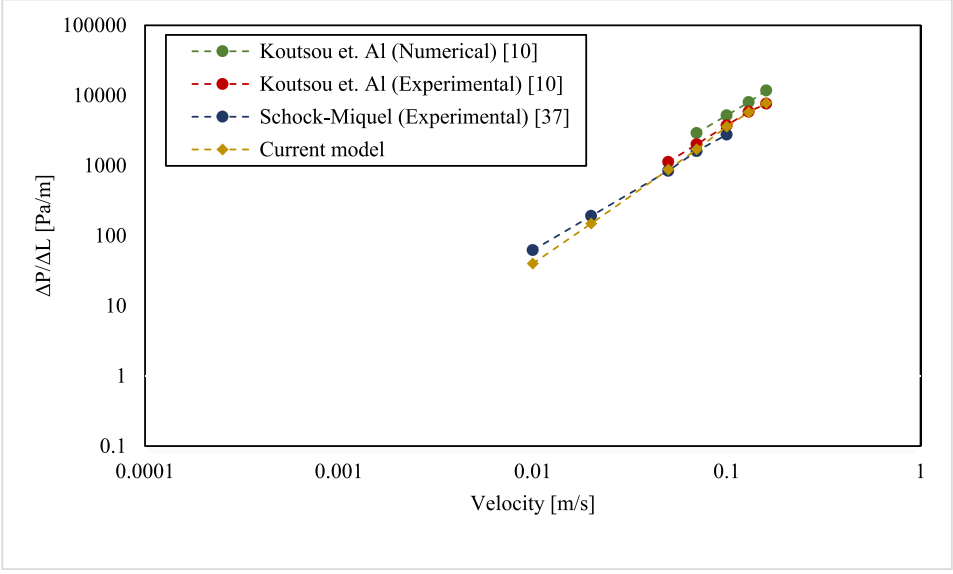

Fig. 6. Comparison of the current model predictions from this work with previous data [10,37] in case of channel incorporated with spacers of Cylinder 90^0.

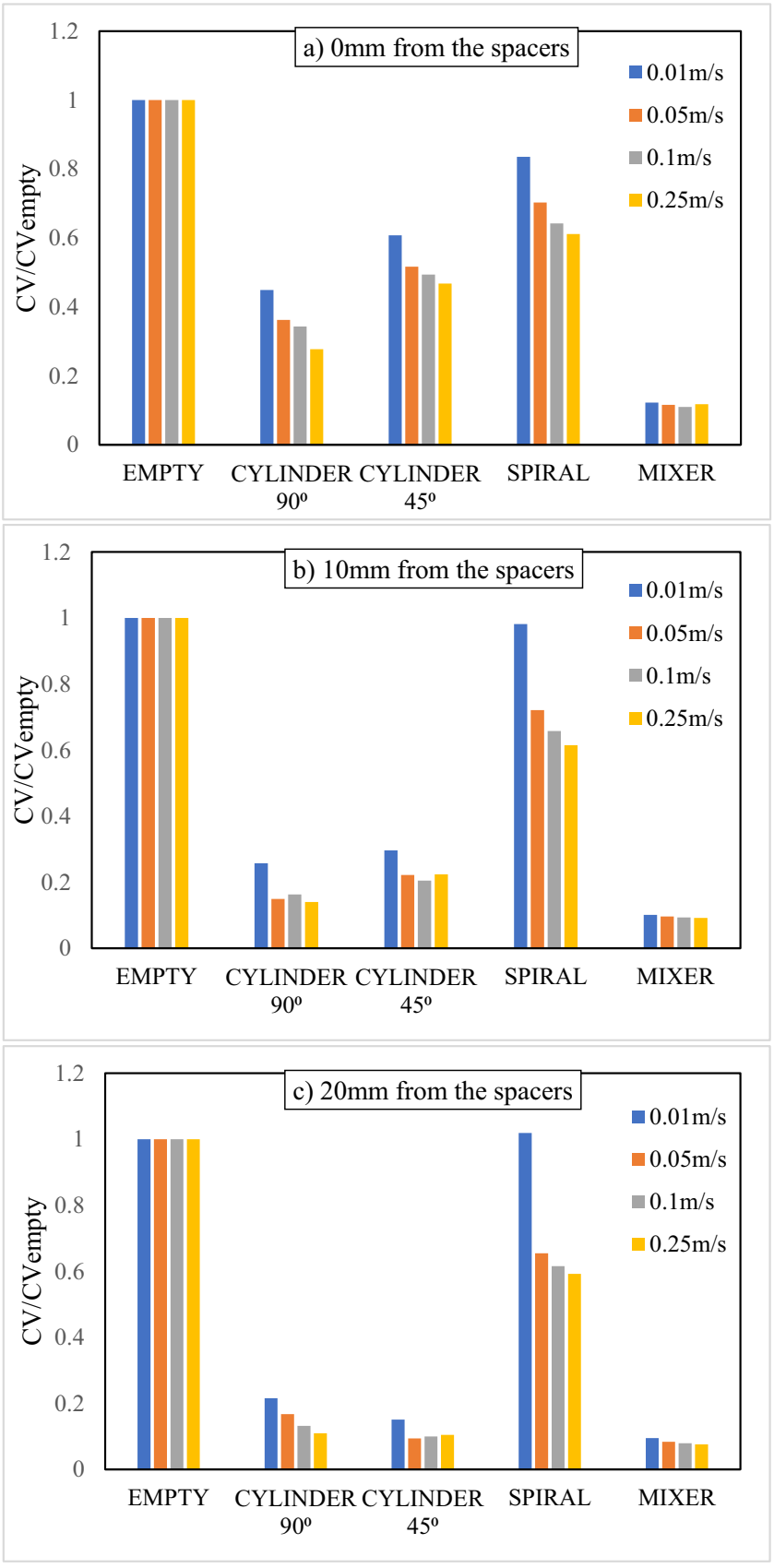

Fig. 7. CV ratio for the various geometry spacers.

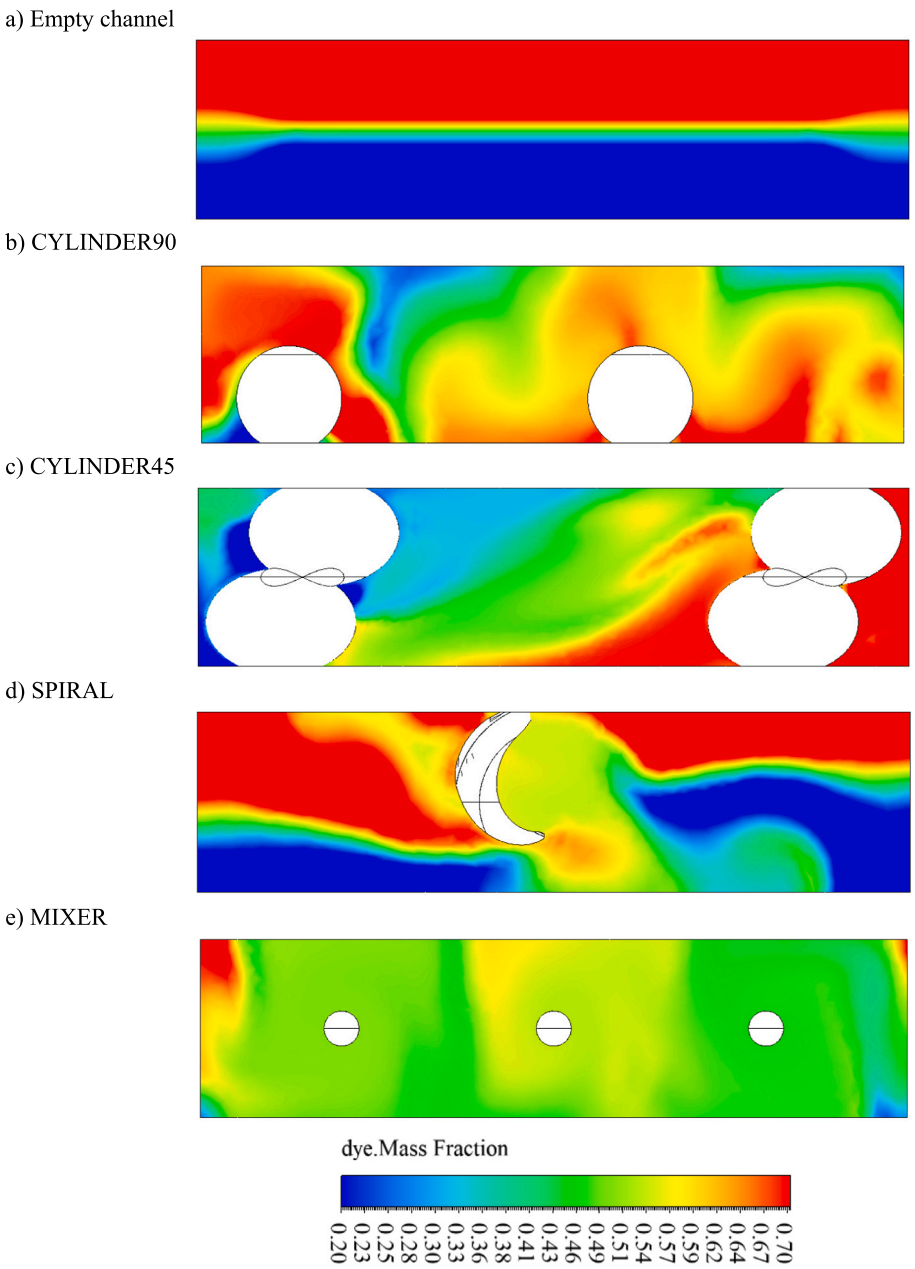

Fig. 8. Contours of dye mass fraction for a) the empty channel, b) channel with Cylinder 90^0, c) Cylinder 45^0, d) Spiral, and e) mixer spacers, at an inlet flow velocity of 0.25 m/s.

20 mm distance from the spacer. In contrast, for spiral and mixer spacers, there is minimal variation in mixing behavior under the same conditions.

In summary, the results indicate that major enhancements in mixing behavior can be achieved over short distances when the mixer spacer is integrated into the system, potentially enabling a more compact module design. Additionally, the graphical representations show that as the flow inlet velocity rises, the effect of including spacers on improving mixing performance becomes stronger. This observation suggests that at higher Reynolds numbers, the impact of the spacers becomes more pronounced in influencing the mixing phenomenon.

To describe the impact of modifying spacer geometries on the mixing behavior mass dye fraction contours on a specific plane perpendicular to the flow direction and located at the end section of the spacers are presented in Fig. 8. It is important to note that at high Reynolds numbers, the convective mixing outweighs the diffusive mixing, and considering the adiabatic nature of the current study, these contours predominantly reflect the influence of the spacers with different geometries.

Observing the contours in the unoccupied channel (Fig. 8a), minimal mixing is observed, primarily due to the exceedingly low mass diffusivity at the fluid interface. In the cases involving cylindrical spacers (Fig. 8b,c), a moderate distribution of dye fraction was observed. Conversely, the implementation of the spiral spacer (Fig. 8d), led to the least uniform distribution of dye. However, the utilization of the mixer spacer (Fig. 8e) resulted in a remarkably efficient mixing process, as evidenced by the well-distributed dye fraction.

Furthermore, the coefficient of variation (CV) is computed at various perpendicular planes to the flow direction located at different distances (0, 5, 10, 15, and 20 mm) away from the endpoint of the spacers for the range of the flow inlet velocity studied, aiming to assess the extent to which mixing is enhanced for each spacer geometry, Fig. 9. The plane of 0 mm distance represents the plane at the end of a spacer which is used to visualize the dye mass fraction contours in Fig. 8.

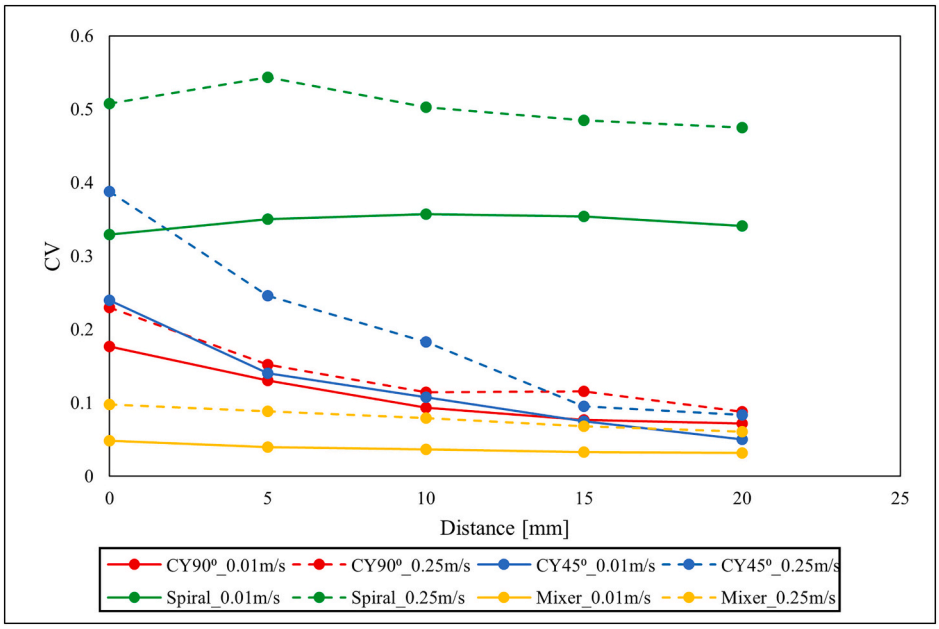

Fig. 9. CV against distance from the end of the spacer geometries.

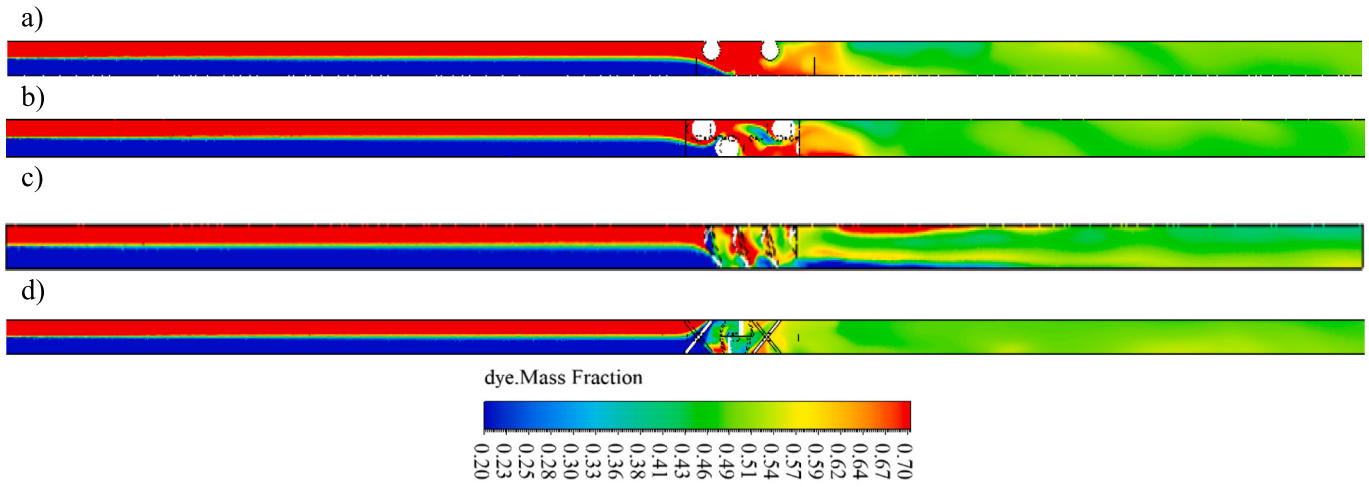

Fig. 10. Contours of dye mass fraction for a plane placed in the middle of the channel and parallel to the flow direction: a) channel with Cylinder 90^0, b) Cylinder 45^0, c) Spiral, and d) mixer spacers, at an inlet flow velocity of 0.25 m/s.

It can be observed that in the case of the mixer spacer, the CV slightly decreases along the distance. Therefore, there is no big change in the mixing behavior of the fluids along the channel, as it already achieves a high level of mixing performance by the end of the spacer.

In contrast, for the Cylinder 90^0 and Cylinder 45^0 spacers, a notable decrease in CV is observed as the distance from the spacer increases. Also, at a distance of 20 mm from the spacers, both types of cylindrical spacers exhibit a considerable improvement in acting as mixer spacers, leading to enhanced mixing processes. On the other hand, for the spiral spacer configuration, there is no significant enhancement further away from the spacer. This observation is supported by comparing dye mass fraction contours presented in Fig. 10.

Fig. 11 provides an analysis of the impact of the various geometry spacers on pressure drop within the system. The results indicate that the empty channel consistently exhibits the lowest pressure drop, resulting in lower pumping energy consumption for the overall process. The pressure drop in the empty channel ranges from 0.07 to 17.76 Pa. The introduction of a spacer as a turbulence promoter in the channel leads to a concurrent increase in the necessary pumping power. This rise is attributed to multiple factors, including the frictional resistance generated by the presence of the spacer, as well as the occurrence of flow instabilities such as eddies or vortices, and disrupting the boundary layer. These combined effects contribute to the loss of pressure along the channel. Among the spacer geometries, Cylinder 45^0 induces the highest pressure drop across all examined velocities. Conversely, the spiral spacer exhibits the lowest pressure drop, ranging from 0.13 to 44.8 Pa. Furthermore, the graph reveals an increasing trend in pressure drop for the spacers as the flow velocity at the inlet rises.

Across all examined spacer geometries, the findings consistently demonstrate a negative correlation between pressure drop and mixing performance. This relationship is demonstrated in Fig. 12, which is non-linear in all situations but shows that a rise in pressure drop is correlated with an increase in the CV. The spiral spacer exhibits behavior closest to that of an empty channel in terms of energy consumption, while still offering poor mixing performance within the system. Therefore, the simultaneous optimization of both parameters still necessitates

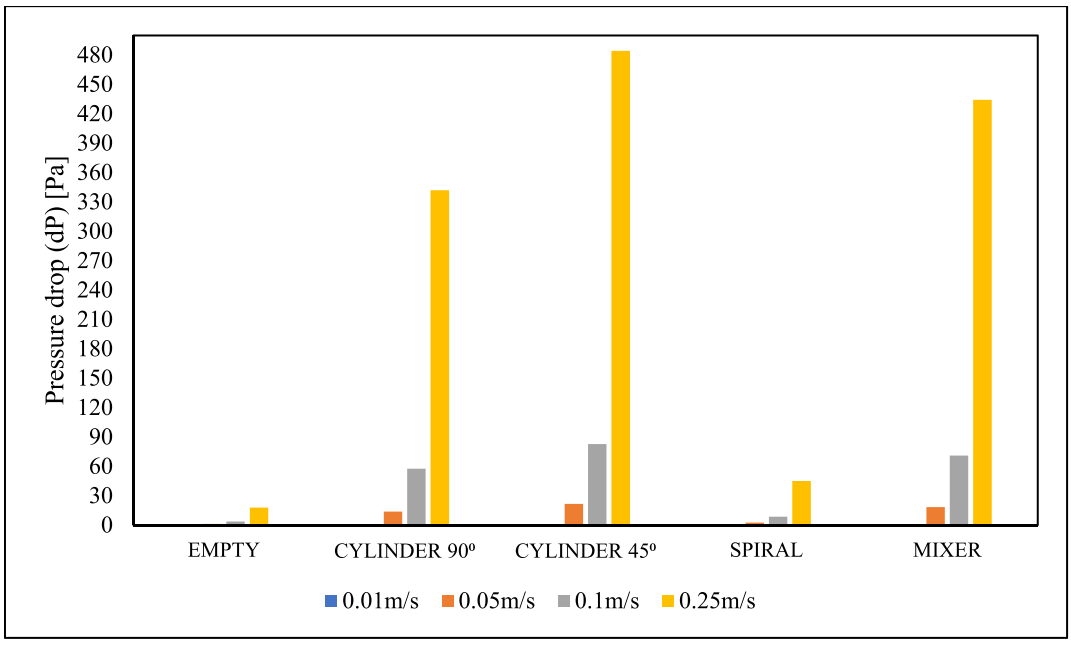

Fig. 11. Pressure drop for the various geometry spacers.

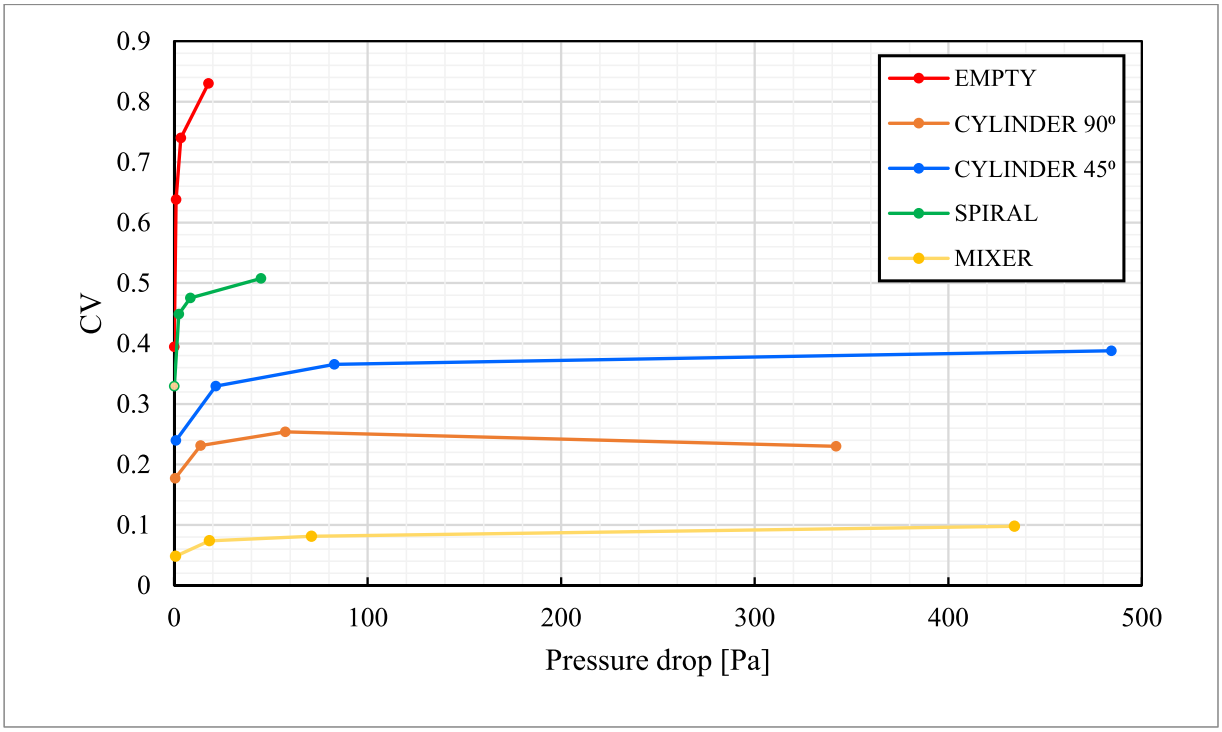

Fig. 12. CV of Various Spacers vs. Pressure Drop.

additional exploration of novel designs.

3.1.2. *Effect of spacer voidage*

Pressure drop values are plotted against spacers' voidage of different geometries in Fig. 13, where Cylinder 90^0 is plotted as (●), Cylinder 45^0 (●), Spiral (●), and Mixer (●). The analysis reveals that, for the examined geometries and the given inlet velocities of 0.01 m/s and 0.25 m/s, there is no statistically significant association between these variables. Thus, it is evident that the variance in pressure drop is primarily linked to the variations in geometry rather than solely differences in spacer occupancy.

3.1.3. *Effect of spacer design variation*

A sensitivity analysis was conducted to examine the impact of geometrical parameters, specifically the inclination angle of the spiral wall and the revolution of the spiral, on the performance of the spacers (see Fig. 14). Notably, it was observed that increasing the number of revolutions in the spiral geometry led to a slight reduction in the coefficient of variation (CV), indicating a slight improvement in mixing performance. Conversely, the pressure drop rises proportionally with an

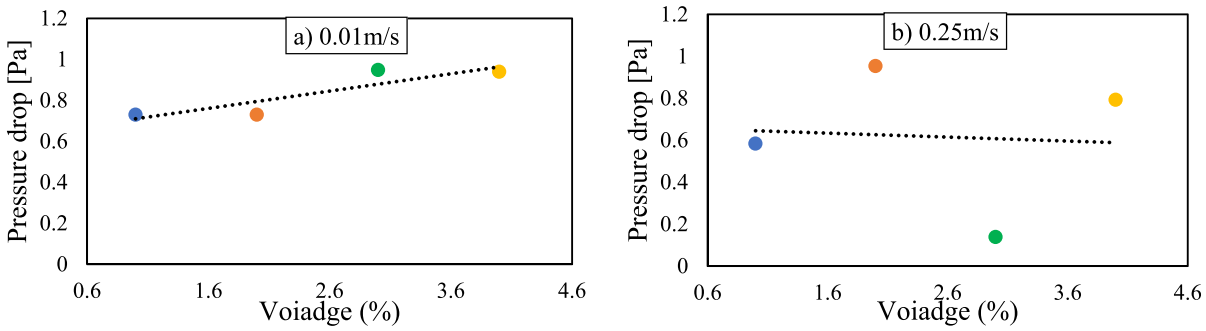

Fig. 13. Pressure drop against spacers' voidage at flow inlet velocities (a) 0.01 m/s (b) 0.25 m/s.

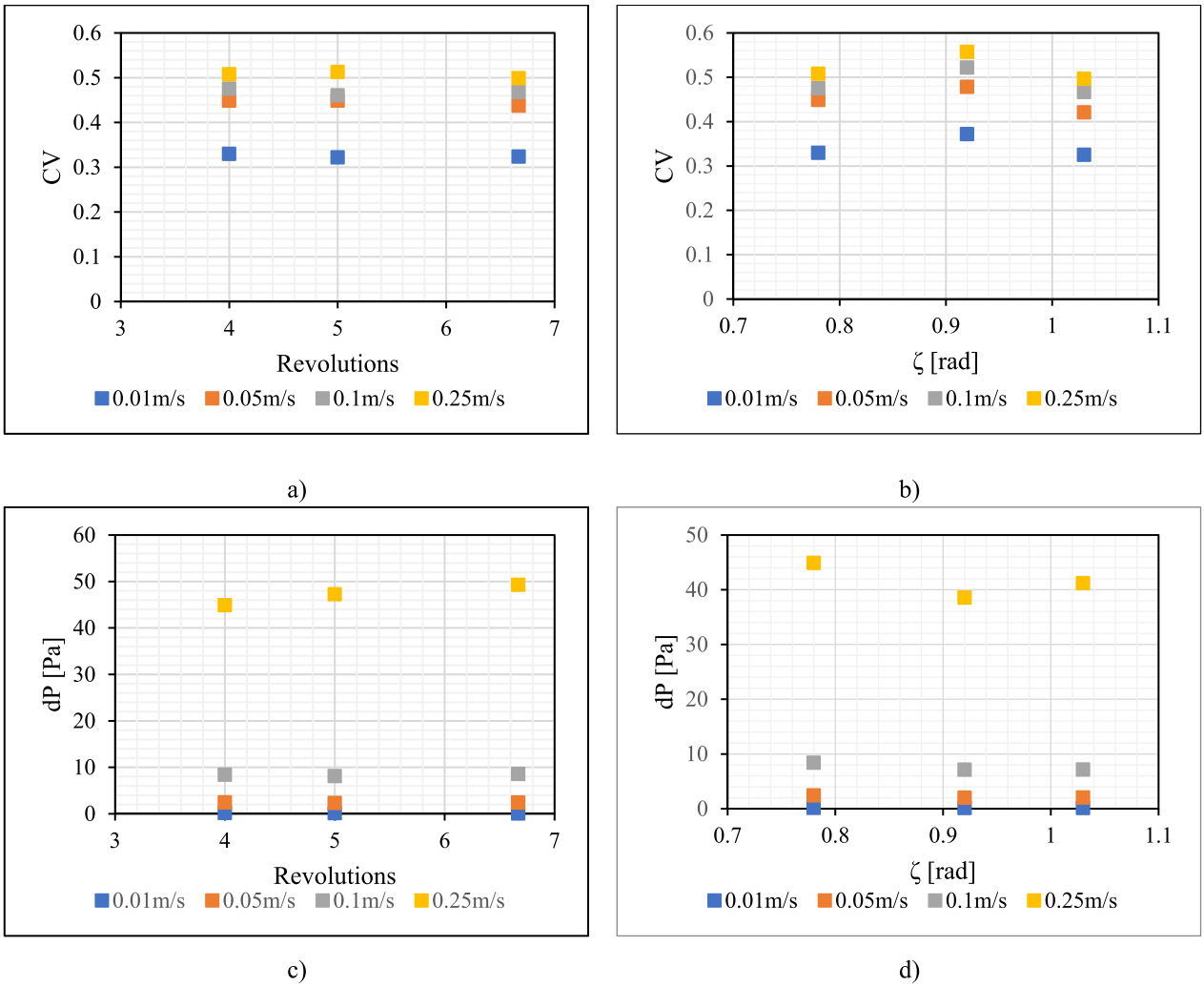

Fig. 14. Impact of revolutions and wall inclination angle on the spacer performances.

increasing number of revolutions. On the other hand, the CV displayed a parabolic relationship with the inclination angle, while the pressure drop demonstrated a decline in values as the inclination angle increased. Furthermore, it was noted that changes in geometry had a more pronounced impact at higher speeds on the mixing process.

3.1.4. Effect of salinity on the mixing performance

Within the context of AGMD, seawater serves as the predominant fluid. Fig. 15 the coefficient of variation (CV) values corresponding to different salinity levels (ranging from 0 g/kg to 120 g/kg) at the termination of each spacer. In this framework, S0 signifies the fluid characterized by properties similar to those of pure water, following the baseline investigation. The thermophysical characteristics of seawater are delineated in Sharqawy et al.'s work [38]. Analysis of the outcomes reveals that in the case of a channel featuring a mixer spacer, the degree of fluid mixing remains consistent across all salinity ranges investigated (S0-S120). Meanwhile, for alternative spacer geometries, the CV values exhibit a remarkable degree of uniformity with negligible discrepancies observed in select cases. In conclusion, the findings of this study indicate that water with a salinity level of up to 120 g/kg demonstrates nearly

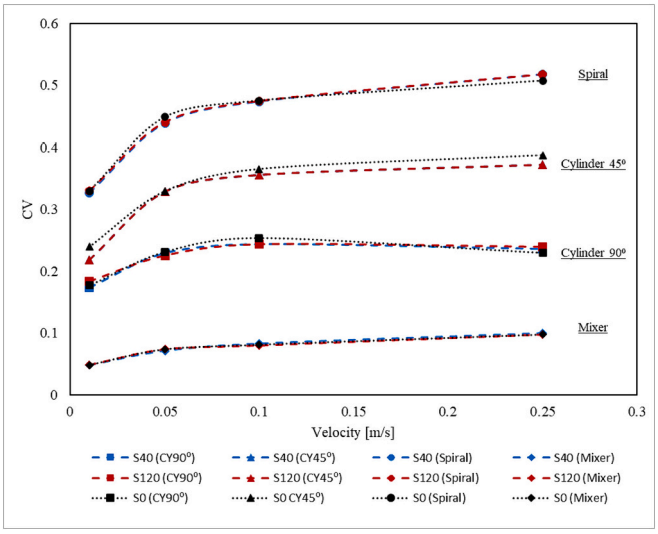

Fig. 15. CV against the fluid inlet velocity, water salinity range (0−120) g/kg.

identical mixing behavior. The incremental changes in water density and viscosity resulting from increased salinity exert only a minor effect on the overall mixing process.

3.2. Heat transfer study

3.2.1. Effect of spacer geometry on Nusselt number

The study investigates the thermal interaction between a hot fluid stream and a membrane in a hot channel. Nusselt numbers (*Nu*) representing convective heat transfer on the membrane's wall are numerically computed and presented in Fig. 16. The mixer geometry excels at lower velocities (0.01 m/s and 0.05 m/s), showing a substantial 30 % and 197 % increase in *Nu* compared to the empty channel. Conversely, the Cylinder 45^0 geometry performs best at higher velocities (0.1 m/s and 0.25 m/s), with *Nu* enhancements of 112 % and 65 %, respectively. Among spacer geometries, the Spiral geometry exhibits the lowest heat transfer performance, with *Nu* values enhancing by 6 %, 20 %, 24 %, and 9 % across the flow velocity range.

3.2.2. Effect of spacer geometry on temperature distribution and flow velocity

The temperature distribution within the hot channel for the working fluid constitutes a significant concern, serving as a crucial indicator of the ongoing heat transfer process. Fig. 17 shows the temperature distribution for the water flow in a plane placed in the middle of the hot channel with and without the conducted spacer configurations at inlet flow velocities of 0.01 m/s and 0.25 m/s. Better temperature distributions are shown in the case of the mixer geometry, characterized by more uniform heat dispersion and less presence of notable hot spots or cold spots. Flow velocity contours are presented in Fig. 18 for various spacer configurations studied, in comparison to the empty channel, focusing on inlet flow velocities of 0.01 m/s and 0.25 m/s. The graphs display the flow disturbances occurring after the introduction of the spacer geometries, which effectively contribute to the enhancement of the heat transfer process within the channel. In particular, reducing wake production is essential for promoting heat transfer. Comparing the velocity contours in Fig. 18(C,e, E,c), it can be observed that the mixer spacer exhibits the highest Nusselt number (*Nu*) at lower velocities, while the Cylinder 45^0 spacer demonstrates better heat transfer performance at higher velocities, exceeding the conventional Cylinder 90^0 spacer.

3.3. Assessing spiral and mixer spacers performance

Fig. 19 presents a performance comparison between the spiral and mixer geometries and the traditional 90^0 cylinder configuration. For each parameter (dP, CV, and *Nu*), the performance change is calculated as a difference between its value for spiral, mixer, and cylinder 90^0 cases, normalized against the value for cylinder 90^0 case. In other words, it is a percentage of change compared to the standard cylinder 90^0 geometry.

The spiral spacer demonstrates a noteworthy reduction of approximately 83 % in pressure drop compared to the cylinder 90° spacer. However, it exhibits notably higher CV values, approximately 97 % more, which correlates to a proportional decrease of mixing performance by the same percentage, and the Nusselt number (*Nu*) experiences a reduction of approximately 20 %. (Fig. 17a).

Conversely from Fig. 17b, the mixer spacer exhibits a pressure drop approximately 30 % higher than the cylinder 90° spacer, while concurrently reducing the CV by approximately 67 %. This reduction in

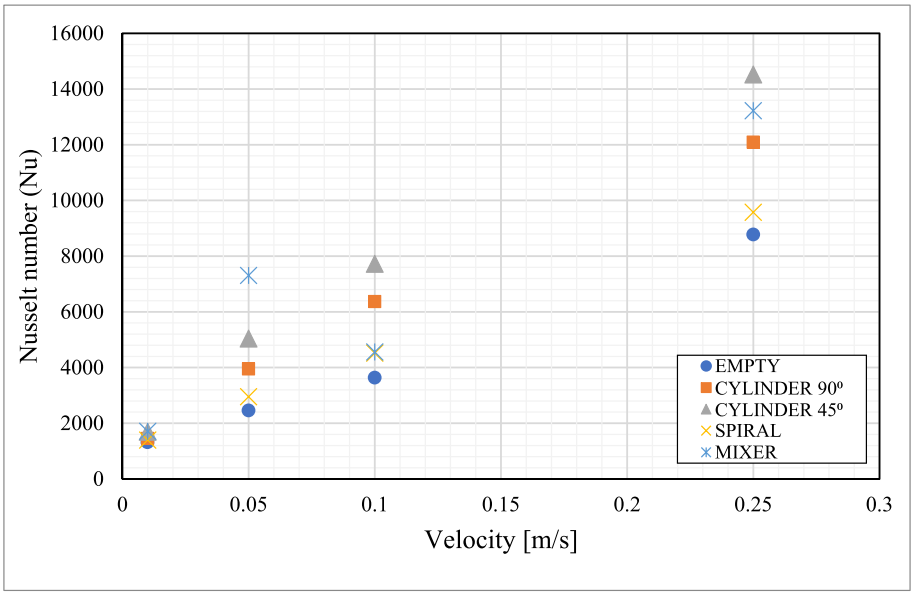

Fig. 16. Nusselt number values for the various spiral geometry.

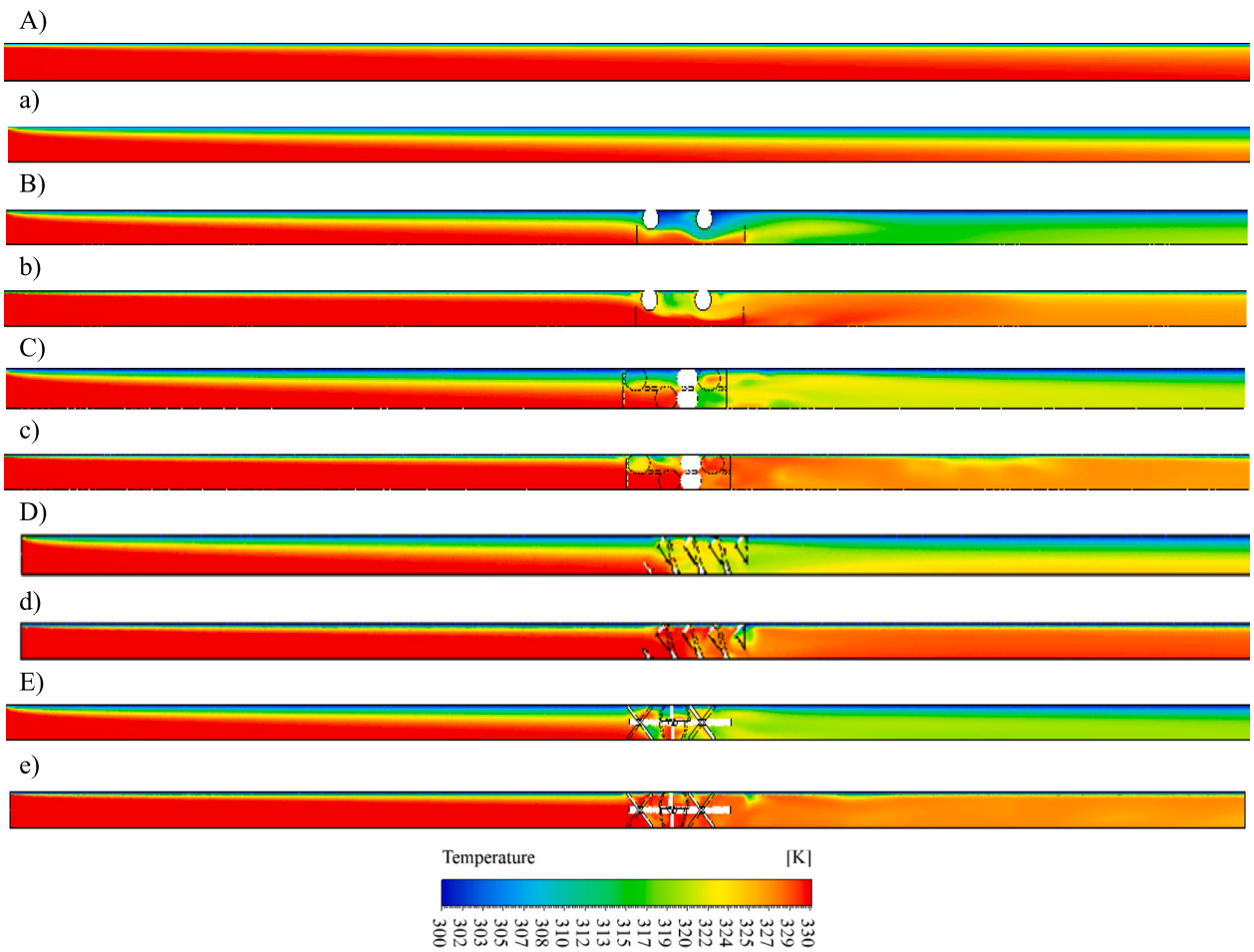

Fig. 17. Contours of Temperature for the empty channel, channel with Cylinder 90^0, Cylinder 45^0, Spiral, and mixer spacers, at an inlet flow velocity of 0.01 m/s for (A, B,C, D,E) and 0.25 m/s for (a,b,c,d,e).

CV indicates a corresponding enhancement of mixing performance by the same percentage, coupled with an improvement in the Nusselt number by approximately 21 %.

In light of the comprehensive evaluation of mixing and heat transfer efficacy within the AGMD system, it is advisable to integrate a mixer geometry spacer in the hot channel to enhance freshwater production. This spacer geometry demonstrates improved outcomes in both mixing performances, considered a proxy for mass transfer in this investigation, and heat transfer performance, as quantified by the Nusselt number (*Nu*). Hence the power required for pumping is negligible compared to the heat required in MD processes (as shown by Woldemariam et al. [39]).

4. Conclusions

Based on state-of-the-art of spacer research and industrial static mixer designs two novel spacer geometries have been proposed. Their mixing performance was benchmarked against conventional designs using numerical analysis under a set of flow conditions.

Overall, these two innovative geometries were found to offer advantages in two distinct spacer functions. When the spacer primarily serves as a structural component, minimizing pressure drop is crucial. In this scenario, the spiral geometry was demonstrated to be the most suitable due to its ability to generate the lowest pressure drop. On the other hand, when improved mixing and heat transfer are the main spacer purpose, the increased pumping energy expenditure is of secondary importance. In this scenario, the *mixer* geometry was shown to be the most suitable.

Moreover, details of a specific geometry design greatly impact mixing performances, as shown by the investigation of spiral geometry variations. Therefore, further research should be dedicated to optimizing the promising designs.

To deepen the analysis, another performance indicator was introduced by Chernyshov et al. [16], defining a spacer efficiency:

$$E = \frac{F}{dP/L}$$

where F is the ratio between the transmembrane flux (F), and (dP/L) is the pressure drop among the channel length. A channel without a spacer is always the most energy efficient. However, an empty channel also provides the least permeate flux at a given Reynolds number. Thus, a complete life cycle analysis of the membrane and spacer production would be of great interest to decide whether smaller devices with greater energy requirements are overall more energy efficient than bigger devices with smaller energy demand.

CRediT authorship contribution statement

Alaa Adel Ibrahim: Writing – original draft, Visualization, Validation, Software, Methodology, Investigation, Data curation. **Marie-Alix Dalle:** Writing – original draft, Software, Methodology, Investigation, Conceptualization. **Filip Janasz:** Writing – review & editing, Supervision. **Stephan Leyer:** Writing – review & editing, Supervision, Project administration.

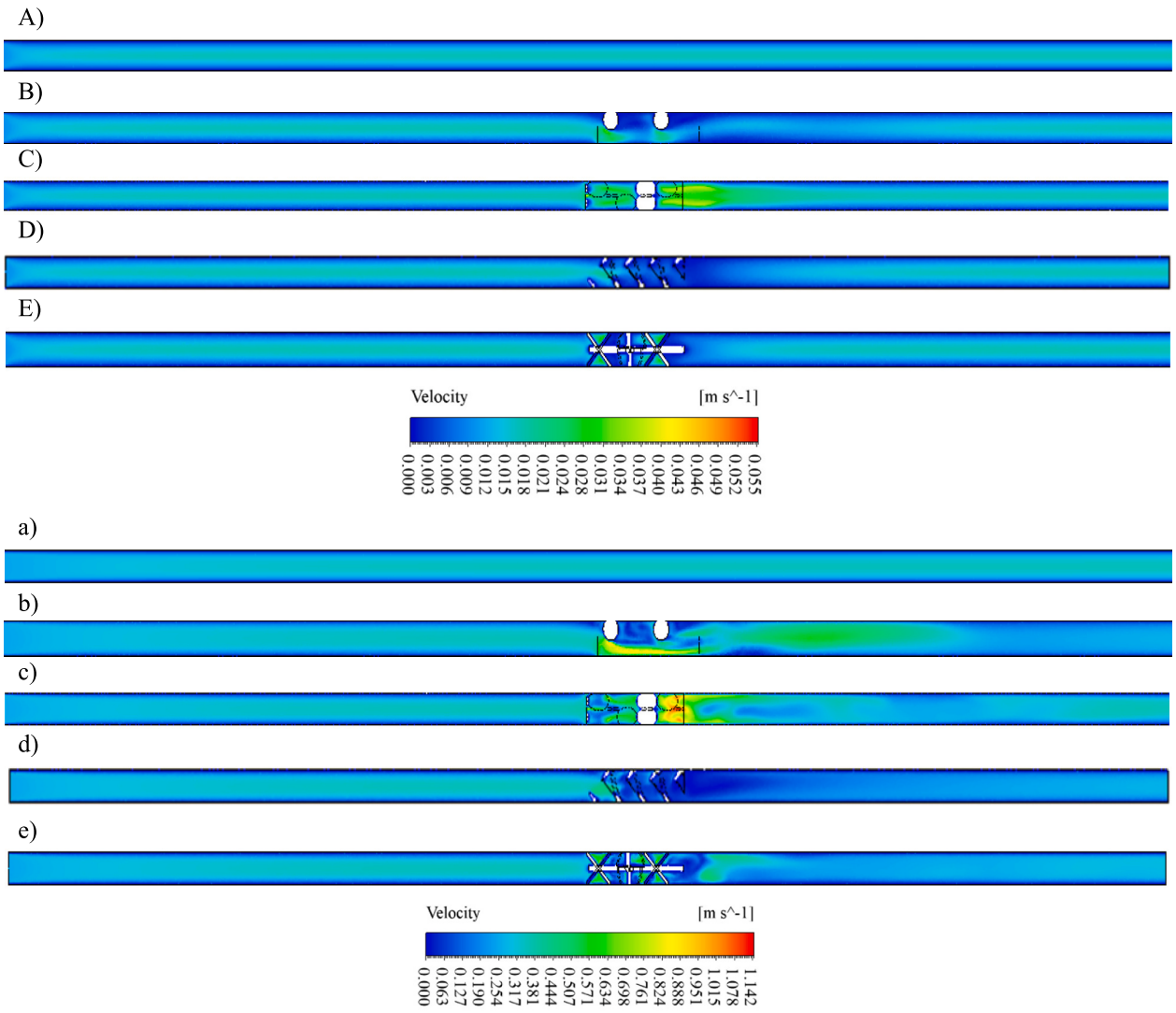

Fig. 18. Contours of Velocity for the empty channel, channel with Cylinder 90^0, Cylinder 45^0, Spiral, and mixer spacers, at an inlet flow velocity of 0.01 m/s for (A,B, C,D,E) and 0.25 m/s for (a,b,c,d,e).

Declaration of competing interest

Alaa Adel Ibrahim reports financial support was provided by FNR - Luxembourg National Research Fund. The remaining authors declare that they have no known competing financial interests or personal relationships that could have appeared to influence the work reported in this paper.

Data availability

The data that has been used is confidential.

Appendix A. Governing equations

Mass conservation:

$$\frac{\partial \rho}{\partial t} + \vec{\nabla} \cdot \rho \vec{V} = 0 \tag{1}$$

where t is the time and p is the density.

Momentum conservation:

$$\rho \left[\frac{\partial \left(\vec{V} \right)}{\partial t} + \vec{V} \bullet \nabla \vec{V} \right] = -\nabla p + \mu \nabla^2 \vec{V} + \frac{1}{3} \mu \nabla \left(\nabla \bullet \vec{V} \right) + \overrightarrow{F_b} \tag{2}$$

a)

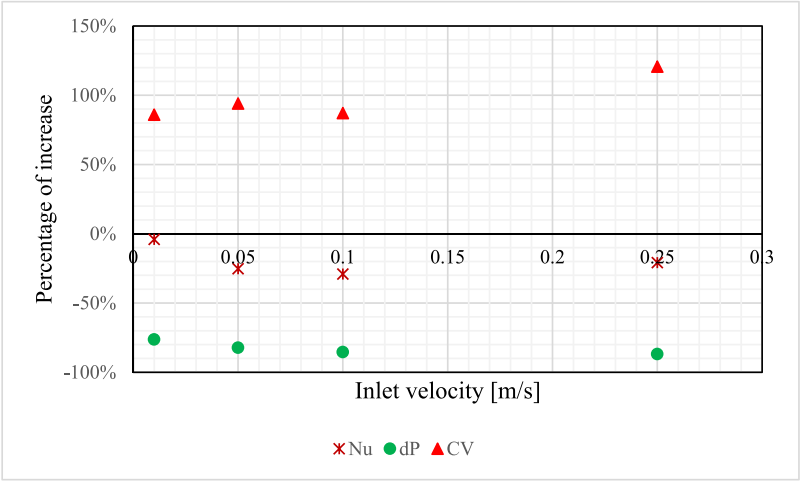

b)

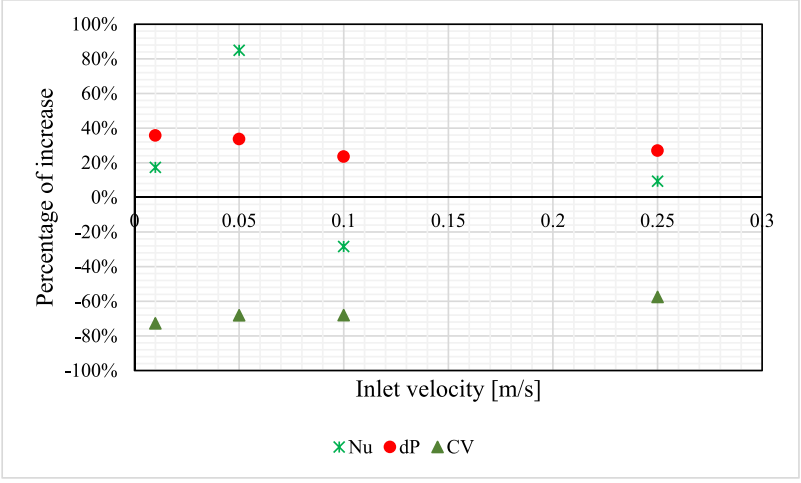

Fig. 19. Comparison of a) Spiral, b) Mixer geometries calculated dP, CV, and *Nu* values to those of cylinder 90^0.

where μ is the viscosity and F_b is the body force.

Energy conservation:

$$\frac{\partial(\rho e_t)}{\partial t}+\nabla.\left[\overrightarrow{V}\ (\rho e_t+p)\right]=\nabla.\left[k\nabla T+\left(\overrightarrow{\tau}\bullet\overrightarrow{V}\right)\right]+S_g \tag{3}$$

where $\overrightarrow{\tau}$ is the shear stress tensor, and S_g is the generated source term.

The shear-Stress Transport (SST) k-ω Model describes the characteristics of turbulence within fluid flow by means of two transport equations.

For turbulent kinetic energy k,

$$\frac{\partial}{\partial t}(\rho k)+\frac{\partial}{\partial x_i}(\rho k u_i)=\frac{\partial}{\partial x_j}\left(\Gamma_k\frac{\partial k}{\partial x_j}+G_k-Y_k+S_k\right) \tag{4}$$

and for the specific turbulent dissipation rate ω,

$$\frac{\partial}{\partial t}(\rho\omega)+\frac{\partial}{\partial x_i}(\rho\omega u_i)=\frac{\partial}{\partial x_j}\left(\Gamma_\omega\frac{\partial\omega}{\partial x_j}+G_\omega-Y_\omega+D_\omega+S_\omega\right) \tag{5}$$

where G_k and G_ω are the generation of turbulence kinetic energy and ω, Γ_k and Γ_ω represent the effective diffusivity of k and ω, respectively. Y_k and Y_ω represent the dissipation of k and ω due to turbulence. D_ω is the cross-diffusion term. S_k and S_ω are source terms.

References

[1] L. Francis, F.E. Ahmed, N. Hilal, Advances in membrane distillation module configurations, Membranes 12 (2022) 81, https://doi.org/10.3390/membranes12010081.

[2] L. Chen, P. Xu, H. Wang, Interplay of the factors affecting water flux and salt rejection in membrane distillation: a state-of-the-art critical review, Water 12 (10) (2020) 2841, https://doi.org/10.3390/w12102841.

[3] H. Abulkhair, I.A. Moujdin, B. Kaddoura, M.S. Khan, Fouling mitigation in membrane distillation using pulsation flow technique, Processes 11 (9) (2023) 2759, https://doi.org/10.3390/pr11092759.

[4] A. Anvari, A. Azimi Yancheshme, K.M. Kekre, A. Ronen, State-of-the-art methods for overcoming temperature polarization in membrane distillation process: a review, J. Membr. Sci. 616 (2020) 118413, https://doi.org/10.1016/j.memsci.2020.118413.

[5] F. Li, W. Meindersma, A.B. de Haan, T. Reith, Novel spacers for mass transfer enhancement in membrane separations, J. Membr. Sci. 253 (2005) 1–12, https://doi.org/10.1016/j.memsci.2004.12.019.

[6] M.U. Farid, J.A. Kharraz, C.-H. Lee, J.K.-H. Fang, S. St-Hilaire, A.K. An, Nanobubble-assisted scaling inhibition in membrane distillation for the treatment of high-salinity brine, Water Res. 209 (2022) 117954, https://doi.org/10.1016/j.watres.2021.117954.

[7] L. Liu, Z. Xiao, Y. Liu, X. Li, H. Yin, A.V. Volkov, T. He, Understanding the fouling/scaling resistance of superhydrophobic/omniphobic membranes in membrane distillation, Desalination 499 (2021) 114864, https://doi.org/10.1016/j.desal.2020.114864.

[8] W. Ni, Y. Li, G. Zhang, X. Du, Study of spacer structure on the enhancement of heat and mass transfer in direct contact membrane distillation modules, Desalination 530 (2022) 115617, https://doi.org/10.1016/j.desal.2022.115617.

[9] A. Hagedorn, G. Fieg, D. Winter, J. Koschikowski, A. Grabowski, T. Mann, Membrane and spacer evaluation with respect to future module design in membrane distillation, Desalination 413 (2017) 154–167, https://doi.org/10.1016/j.desal.2017.03.016.

[10] C.P. Koutsou, S.G. Yiantsios, A.J. Karabelas, Direct numerical simulation of flow in spacer-filled channels: effect of spacer geometrical characteristics, J. Membr. Sci. 291 (2007) 53–69, https://doi.org/10.1016/j.memsci.2006.12.032.

[11] A.R. Da Costa, A.G. Fane, D.E. Wiley, Spacer characterization and pressure drop modelling in spacer-filled channels for ultrafiltration, J. Membr. Sci. 87 (1994) 79–98, https://doi.org/10.1016/0376-7388(93)E0076-P.

[12] K. Ali, H.A. Arafat, M.I.H. Ali, Detailed numerical analysis of air gap membrane distillation performance using different membrane materials and porosity, Desalination 551 (2023) 116436, https://doi.org/10.1016/j.desal.2023.116436.

[13] M. Rabie, A.Y.M. Ali, E.M. Abo-Zahhad, H.I. Elqady, M.F. Elkady, S. Ookawara, A. H. El-Shazly, M.S. Salem, A. Radwan, Thermal analysis of a hybrid high concentrator photovoltaic/membrane distillation system for isolated coastal regions, Sol. Energy 215 (2021) 220–239, https://doi.org/10.1016/j.solener.2020.12.029.

[14] Z. Xu, Y. Pan, Y. Yu, CFD simulation on membrane distillation of NaCl solution, Front. Chem. Eng. China 3 (2009) 293–297, https://doi.org/10.1007/s11705-009-0204-7.

[15] F. Li, G.W. Meindersma, A.B. de Haan, T. Reith, Optimization of non-woven spacers by CFD and validation by experiments, Desalination 146 (2002) 209–212, https://doi.org/10.1016/S0011-9164(02)00472-1.

[16] M.N. Chernyshov, G.W. Meindersma, A.B. de Haan, Comparison of spacers for temperature polarization reduction in air gap membrane distillation, Desalination 183 (2005) 363–374, https://doi.org/10.1016/j.desal.2005.04.029.

[17] J. Seo, Y.M. Kim, J.H. Kim, Spacer optimization strategy for direct contact membrane distillation: shapes, configurations, diameters, and numbers of spacer filaments, Desalination 417 (2017) 9–18, https://doi.org/10.1016/j.desal.2017.05.009.

[18] S. Al-Sharif, M. Albeirutty, A. Cipollina, G. Micale, Modelling flow and heat transfer in spacer-filled membrane distillation channels using open source CFD code, Desalination 311 (2013) 103–112, https://doi.org/10.1016/j.desal.2012.11.005.

[19] M. Shakaib, S.M.F. Hasani, I. Ahmed, R.M. Yunus, A CFD study on the effect of spacer orientation on temperature polarization in membrane distillation modules, Desalination 284 (2012) 332–340, https://doi.org/10.1016/j.desal.2011.09.020.

[20] D. Dendukuri, S.K. Karode, A. Kumar, Flow visualization through spacer filled channels by computational fluid dynamics-II: improved feed spacer designs, J. Membr. Sci. 249 (2005) 41–49, https://doi.org/10.1016/j.memsci.2004.06.062.

[21] W. Ni, Y. Li, G. Zhang, X. Du, Study of spacer structure on the enhancement of heat and mass transfer in direct contact membrane distillation modules, Desalination 530 (2022) 115617, https://doi.org/10.1016/j.desal.2022.115617.

[22] S. Armbruster, F. Stockmeier, M. Junker, M. Schiller-Becerra, S. Yüce, M. Wessling, Short and spaced twisted tapes to mitigate fouling in tubular membranes, J. Membr. Sci. 595 (2020) 117426, https://doi.org/10.1016/j.memsci.2019.117426.

[23] M.M. Haddadi, S.H. Hosseini, D. Rashtchian, M. Olazar, Comparative analysis of different static mixers performance by CFD technique: an innovative mixer, Desalination 28 (2020) 672–684, https://doi.org/10.1016/j.cjche.2019.09.004.

[24] Sudhanshu S. Soman, Chandra Mouli R. Madhuranthakam, Effects of internal geometry modifications on the dispersive and distributive mixing in static mixers, Chem. Eng. Process. Process Intensif. 122 (2017) 31–43, https://doi.org/10.1016/j.cep.2017.10.001.

[25] Paul Gramann, Bruce Davis, A new dispersive and distributive static mixer for the compounding of highly viscous materials, Mater. Sci. Eng. (1999).

[26] R.K. Thakur, C. Vial, K.D.P. Nigam, E.B. Nauman, G. Djelveh, Static mixers in the process industries—a review, Chem. Eng. Res. Des. 81 (2003) 787–826, https://doi.org/10.1205/026387603322302968.

[27] J. Liu, A. Iranshahi, Y. Lou, G. Lipscomb, Static mixing spacers for spiral wound modules, J. Membr. Sci. 442 (2013) 140–148, https://doi.org/10.1016/j.memsci.2013.03.063.

[28] A. Shrivastava, S. Kumar, E.L. Cussler, Predicting the effect of membrane spacers on mass transfer, J. Membr. Sci. 323 (2) (2008) 247–256, https://doi.org/10.1016/j.memsci.2008.05.060.

[29] N. Thomas, N. Sreedhar, O. Al-Ketan, R. Rowshan, R.K. Abu Al-Rub, H. Arafat, 3D printed triply periodic minimal surfaces as spacers for enhanced heat and mass transfer in membrane distillation, Desalination 443 (2018) 256–271, https://doi.org/10.1016/j.desal.2018.06.009.

[30] E.H. Cabrera Castillo, N. Thomas, O. Al-Ketan, R. Rowshan, R.K. Abu Al-Rub, L. D. Nghiem, S. Vigneswaran, H.A. Arafat, G. Naidu, 3D printed spacers for organic fouling mitigation in membrane distillation, J. Membr. Sci. 581 (2019) 331–343, https://doi.org/10.1016/j.memsci.2019.03.040.

[31] S. Armbruster, O. Cheong, J. Lölsberg, S. Popovic, S. Yüce, M. Wessling, Fouling mitigation in tubular membranes by 3D-printed turbulence promoters, J. Membr. Sci. 554 (2018) 156–163, https://doi.org/10.1016/j.memsci.2018.02.015.

[32] A. Lévêque, Les Lois de la transmission de chaleur par convection, 1928.

[33] M. Al-Atabi, Design and assessment of a novel static mixer, Can. J. Chem. Eng. 89 (3) (2010) 550–554, https://doi.org/10.1002/cjce.20412.

[34] E. Bennour, C. Kezrane, N. Kaid, S. Alqahtani, S. Alshehery, Y. Menni, Improving mixing efficiency in laminar-flow static mixers with baffle inserts and vortex generators: a three-dimensional numerical investigation using corrugated tubes, Chem. Eng. Process. Process Intensif. 193 (2023) 109530, https://doi.org/10.1016/j.cep.2023.109530.

[35] M. Stec, P.M. Synowiec, Study of fluid dynamic conditions in the selected static mixers part III—research of mixture homogeneity, Can. J. Chem. Eng. 97 (2019) 995–1007, https://doi.org/10.1002/cjce.23290.

[36] J. Xu, Y.B. Singh, G.L. Amy, N. Ghaffour, Effect of operating parameters and membrane characteristics on air gap membrane distillation performance for the treatment of highly saline water 512, 73–82, J. Membr. Sci. (2016), https://doi.org/10.1016/j.memsci.2016.04.010.

[37] Schock, G. and Miquel, A., 1987. Mass transfer and pressure loss in spiral wound modules. Desalination, [online] 64, pp.339–352. doi:https://doi.org/10.1016/0011-9164(87)90107-X.

[38] M.H. Sharqawy, J.H. Lienhard, S.M. Zubair, Thermophysical properties of seawater: a review of existing correlations and data, Desalin. Water Treat. 16 (1–3) (2010) 354–380, https://doi.org/10.5004/dwt.2010.1079.

[39] D. Woldemariam, A. Martin, M. Santarelli, Exergy analysis of air-gap membrane distillation systems for water purification applications, Appl. Sci. 7 (2017) 301, https://doi.org/10.3390/app7030301.